PHYSICAL REVIEW LETTERS

Bifurcation from Bubble to Droplet Behavior in Inviscid Pinch-off

J. C. Burton and P. Taborek

Department of Physics and Astronomy, University of California, Irvine, California, USA

High-speed video is used to analyze the pinch-off of xenon in water. By varying the pressure in the xenon from 0.05 to 68 atm, the mass density ratio $D = \rho_{int}/\rho_{ext}$ of the interior gaseous xenon ρ_{int} to the exterior liquid water ρ_{ext} can be varied by over 3 orders of magnitude. Both the shape of the pinch region and the power law that governs the collapse of the minimum neck radius are distinctly different for the low D (bubblelike) and high D (dropletlike) cases. We show that there is a rather abrupt transition between these types of behavior near $D \approx 0.25$.

The separation of one fluid mass into two disjoined pieces involves the formation of a finite-time singularity in the flow where quantities such as pressure, velocity, and curvature diverge. A recent review of fluid break-up phenomena can be found in Ref. [1]. This pinch-off process generally involves both an interior and an exterior fluid characterized by different mass densities ρ_{int} and ρ_{ext}, and perhaps other physical properties such as surface tension σ and viscosity η. Viscosity is important at length scales smaller than $\eta^2/(\sigma\rho)$, but for many low viscosity fluids such as air and water, this viscous length is a few nanometers, so most of the pinch-off process can be described as an inviscid flow. Inviscid pinch-off can be characterized by the density ratio $D = \rho_{int}/\rho_{ext}$ where $D \to 0$ corresponds to a low density bubble surrounded by a dense fluid, while the limit $D \to \infty$ corresponds to a dense liquid drop pinching off in a low density vapor. Each of these limiting cases has recently received considerable theoretical and experimental attention. The singularity structure in the droplet case is an example of self-similarity of the first kind, in which singular quantities diverge with power laws with rational exponents; for example, the minimum neck radius of an inviscid droplet scales as $R_{min} \sim (t_0 - t)^{\alpha_{drop}}$, where $\alpha_{drop} = 2/3$ and t_0 is the time at which the singularity occurs [2–9]. In inviscid drop pinch-off, an additional constraint requires the radial and axial lengths to scale in the same way, so the shape of the singular region is preserved, and is universal in the sense that it is independent of initial conditions such as the size of the droplet.

The singularities in bubble pinch-off ($D \to 0$) are qualitatively different. The neck radius has a power-law form $R_{min} \sim (t_0 - t)^{\alpha_{bubble}}$, but $\alpha_{bubble} \approx 1/2$ [10–12]. The shape of the singular region is not constant, but rather evolves from a conical shape to a slender cylinder as the pinch-off proceeds. This evolution takes place over many decades in time, which is related to the fact that α_{bubble} is not strictly constant, but rather has logarithmic corrections [13–16]. Detailed experiments yield an approximate effective exponent with $\alpha_{bubble} \approx 0.53$–0.57 [15,17,18]. Furthermore, bubble pinch-off is extremely sensitive to nonaxisymmet-

ric perturbations [12,18], and retains a memory of the initial conditions.

Pinch-off in both the droplet limit ($D \to \infty$) and bubble limit ($D \to 0$) represents singular asymptotic solutions to the partial differential equations of evolution of the fluid. For dynamical systems described by ordinary differential equations, asymptotic solutions are associated with geometrical objects in the phase space such as fixed points, limit cycles, and strange attractors. For partial differential equations, the phase space is infinite dimensional, but the phase space picture is nevertheless useful for classifying types of singular behavior [19,20]. From the dynamical systems point of view, for each value of the density ratio parameter D there is a fixed point with a basin of attraction and local properties which determine the singular exponents. As D is varied, the properties of the fixed point can vary either smoothly, or abruptly via a bifurcation. The region near both the bubblelike fixed point [16,21] and the dropletlike fixed point [4,7] have been investigated using various numerical techniques, but the nature of the transition from one fixed point to the other has not been explored. In this Letter, we use high-speed video to analyze the pinch-off of xenon from a nozzle submerged in water to experimentally investigate the parameter range $6.5 \times 10^{-4} < D < 0.7$. Xenon is particularly suitable for this purpose because the critical point is slightly below room temperature, so the density can be continuously varied over a wide range with only modest increases in the pressure. At low values of D, pinch-off resembles that of a collapsing vacuum cavity, and at high densities the pinch-off resembles that of a droplet. We observe a sharp increase in the scaling exponent from $\alpha \approx 0.57$ to $\alpha \approx 2/3$ at a density ratio $D \approx 0.25$.

The apparatus consisted of a stainless steel cell filled with water with optical access through two parallel sapphire windows of diameter 3.81 cm and thickness 0.635 cm. The windows were press sealed to the cell with viton o-rings. The xenon emerged from a Teflon nozzle with an inner diameter of 0.47 cm. The nozzle was connected to a high-pressure ($\sim$170 atm) xenon

source. The flow rate of the gas was controlled by a fine
metering valve, so that the bubbles were produced at
approximately 1 bubble per 20 sec. A mechanical vacuum
pump was attached to the cell through a valve so that
subatmospheric pressures could be achieved. The pressure
in the cell could be adjusted from the vapor pressure of
water ($\sim$0.03 atm at 25 °C), to a maximum of 100 atm,
although in practice, we were limited to lower pressures
because xenon forms a solid clathrate with water at room
temperature and tens of atmospheres of pressure [22]. In
order to avoid this problem, all experiments were per-
formed at slightly elevated temperatures ($\sim$37 °C), which
increased the clathrate formation pressure to $P \sim 68$ atm
and allowed us to reach values of $D \approx 0.7$. The pressure
and temperature of the xenon were measured, and the
density was computed from data in Ref. [23]. To obtain a
large dynamic range of measurements of R_{min}, videos were
taken with two levels of optical magnification. For the
images in Fig. 1, the high-speed camera (Phantom v7.2,
Vision Research) was attached to a macro lens, allowing a
full view of the bubble evolution. For the high-
magnification videos in Fig. 2, the camera was attached
to a photographic bellows with a 5 × , long working dis-
tance microscope objective. The optical resolution for this
setup was fixed at 2.4 μm/pixel. Typical frame rates for
the low (high) magnification videos were 40 000
(100 000) fps. All bubble images were captured using
illumination from behind with a 2 μs exposure time.
Back illumination produced bright, white optical artifacts
in the images due to focusing of the light as it passes
through the bubble (Figs. 1 and 2). The images in the
videos were processed so that the minimum neck radius
R_{min} could be measured for each frame. In order to esti-
mate the effects of viscosity during pinch-off, the Reynolds
number Re was calculated using R_{min} and the axial velocity
near R_{min}; the value obtained was Re $\geq$ 100, indicating an
inertia-dominated flow. Images of quiescent bubbles were
used to measure the xenon-water surface tension as a
function of D using axisymmetric drop-shape analysis;
the surface tension varied smoothly from 73 $\pm$
1 dyne/cm at $D = 6.5 \times 10^{-4}$ to 34 $\pm$ 1 dyne/cm at
$D = 0.695$.

Figure 1 shows low-magnification images of the bubble
evolution at four different density ratios. For very low
densities ($D \leq 0.001$), such as in Fig. 1(a), the pinch-off
is nearly perfectly symmetric in the vertical direction. As
the density increases, there is a visible asymmetry in the
vertical direction [Fig. 1(b), 3rd frame]. This is presumably
due to an axial jet of gas from the nozzle into the connect-
ing bubble. As the density is raised even more [Figs. 1(c)
and 1(d)], this asymmetry intensifies until the pinch-off
looks like that of an inverted droplet at $D = 0.7$. After the
initial pinch-off event, the connecting filament begins to
retract towards the nozzle. At higher densities, this filament
can be sufficiently elongated to result in another pinch-off
event prior to retraction, which creates a satellite bubble.
At $D = 0.217$ in Fig. 1(c), the satellite bubble is approxi-
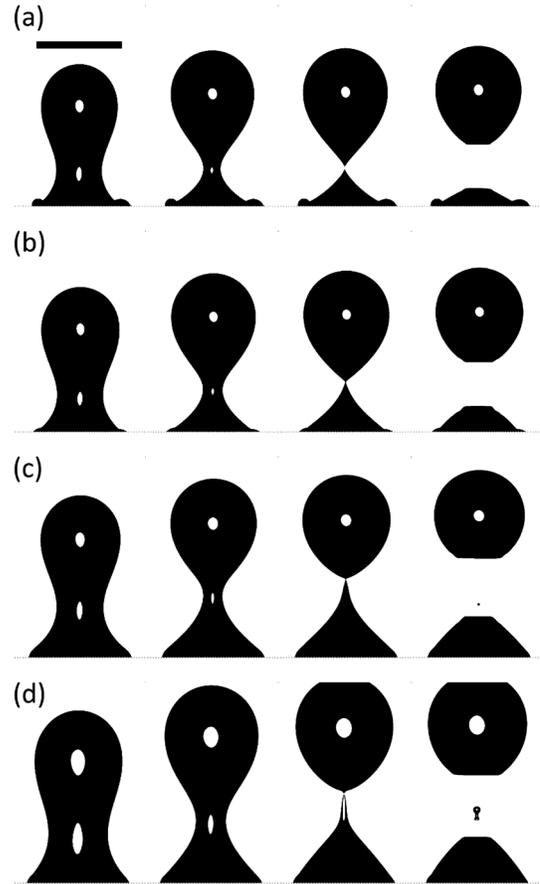

FIG. 1.   Images extracted from the high-speed video showing
the pinch-off of xenon rising in water at four different mass
density ratios (specific gravity): (a) 6.5×10^{-4}, (b) 0.047,
(c) 0.217, (d) 0.695. The scale bar in the first frame of
(a) represents 5 mm, and applies for all images in (a)–(d). The
time stamp on each frame relative to the moment of pinch-off is
(from left to right) (a): -8.95 ms, -1.025 ms, 0 ms, 1.275 ms;
(b): -9.50 ms, -1.35 ms, 0 ms, 1.525 ms; (c): -13.15 ms,
-2.1 ms, 0 ms, 2.6 ms; (d): -58.625 ms, -11.55 ms, 0 ms,
3.225 ms. The bright, white spots in the images are optical
artifacts due to illuminating the bubbles from behind. The
bubbles are larger at higher densities because of decreased
buoyancy as $D \to 1$.

mately 120 μm in diameter and at $D = 0.695$ in Fig. 1(d),
the satellite bubble diameter is 500 μm.

High-magnification images of the upper pinch-off from
the main bubble are shown in Fig. 2 for identical values of
D. At low densities [$D = 6.5 \times 10^{-4}$, 2(a)], the pinch-off
is highly symmetric and collapses very quickly to zero
diameter. The slight rotational asymmetry in the last frame
of Fig. 2(a) is due to the extreme sensitivity to tilts and
perturbations in the nozzle [18]. At slightly higher den-
sities [$D = 0.047$, 2(b)], the pinch-off is less sensitive to
axisymmetric perturbations; however, the vertical symme-
try is lost due to the axial jet of gas flowing into the main
bubble. The increase in vertical asymmetry continues until
the pinch-off geometry finally becomes reentrant [2(d)],
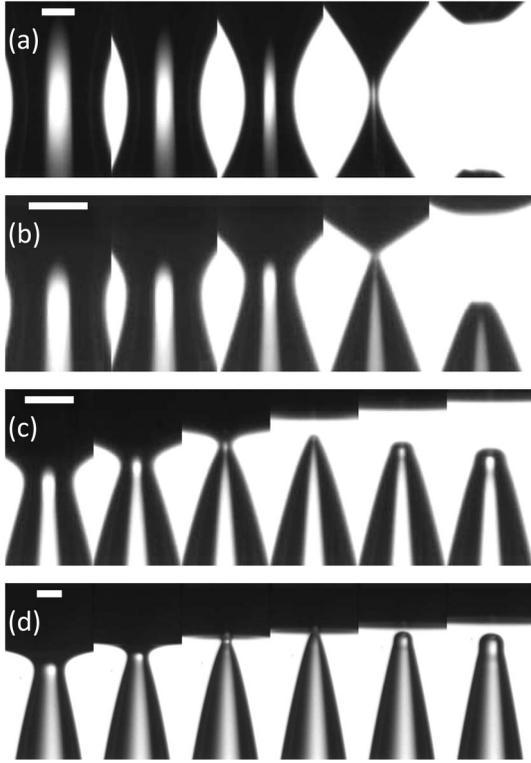where the pinch-off occurs below the optical horizon. This

FIG. 2.   Images extracted from the high-speed video showing
the pinch-off of xenon in water at four different mass density
ratios (specific gravity): (a) 6.5×10^{-4}, (b) 0.047, (c) 0.217,
(d) 0.695. The white bar at the top of the first image in each
sequence represents 100 μm. The time between each successive
image is 30.25 μs, 13 μs, 15 μs, and 20 μs for sequences (a)–
(d), respectively.

is the expected behavior for purely inviscid droplet pinch-
off [3,6,8]. In contrast to previous experimental studies of
bubble pinch-off [12,17,18], we do not observe the creation
of satellite bubbles for $D \leq 0.2$. We note that this differ-
ence may be due to the fact that water used in our experi-
ment was degassed prior to the addition of the xenon. Since
negative pressures develop near the singularity due to high
fluid velocities, dissolved air in water used in [12,17,18]
may have contributed to the creation of satellite bubbles
through nucleation.

   To quantify the transition from bubble to dropletlike
pinch-off, we have measured the minimum neck radius
$R_{\min}$ of the collapsing bubble as a function of time using
a combination of the low and high-magnification video im-
ages. For each value of D, measurements of $R_{\min}$ vs t for
both sets of images were simultaneously fit to the form
$R_{\min} = A(t_0 - t)^{\alpha}$ using a χ^2 method, assuming the same
values of A and α, but a different t_0 for each video. The data
used in the fitting procedure were restricted to values of
$R_{\min}$ for which $(t_0 - t) \leq 200$ μs, since the functional form
is strictly valid only near the singularity [24]. Once the
values of t_0 were determined, the full range of data could
be plotted, as shown in Fig. 3. The minimum and maximum
values of the density ratio $D = 6.5 \times 10^{-4}$ and $D = 0.695$

are unambiguously in the bubblelike and dropletlike re-
gime, respectively, and the power law fits yield values of
the exponents $\alpha_{\text{bubble}} = 0.57$ and $\alpha_{\text{drop}} = 0.66$ in agree-
ment with previous measurements, as shown in Fig. 3(b).

   Figure 4 shows values of the power-law scaling expo-
nent α as a function of the density ratio for values of D that
span the bubblelike and dropletlike regimes. The value and
error estimates for the exponent α were taken from the
fitting procedure, assuming a normally distributed pixel
error with a standard deviation of 0.5 pixels. The error
bars on the values of α represent the 95% confidence
interval from our fitting procedure. α is essentially con-
stant with the value expected for a vacuum bubble $\alpha \approx$
0.57 over a wide range of density ratios until $D \sim 0.1$, at
which point a relatively sharp transition is made to $\alpha \approx$
0.66. The $\alpha = 2/3$ regime is expected to extend indefi-
nitely beyond our maximum value of $D = 0.695$. This has
been experimentally verified for $D \approx 14\,000$ [9].

   For density ratios $D \gtrsim 0.16$ in the droplike regime,
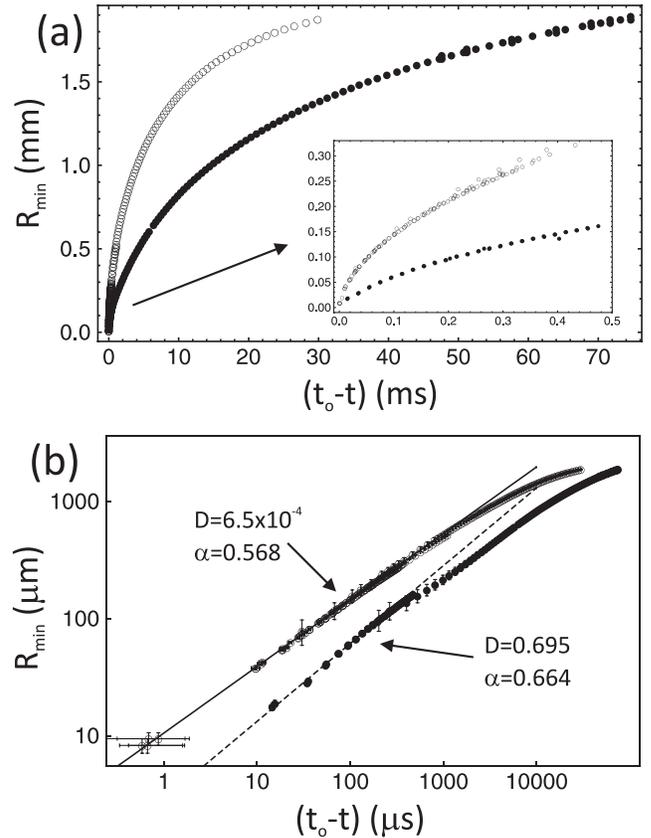boundary-integral numerical simulations of inviscid fluids

FIG. 3.   (a) Linear and (b) $\mathrm{Log}_{10} - \mathrm{Log}_{10}$ plots of $R_{\min}$ vs $(t_0 -
t)$ for a bubblelike density $D = 6.5 \times 10^{-4}$ (open circles) and a
dropletlike density $D = 0.695$ (closed circles). Both sets of data
consist of measurements from one high-magnification video and
multiple low-magnification videos. The inset in (a) shows data
very close to the singular region. Error bars in (b) represent
0.5 pixels in the measurements of $R_{\min}$ and 1 μs in the mea-
surements of $(t_0 - t)$. The solid line in the logarithmic plot rep-
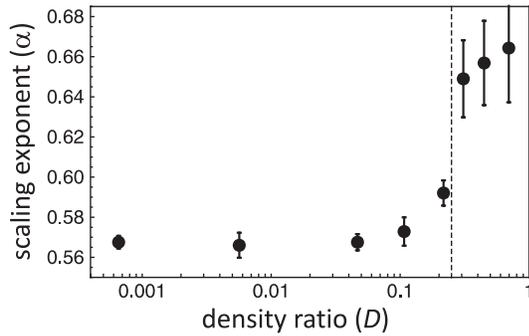resents $(t_0 - t)^{0.568}$ and the dashed line represents $(t_0 - t)^{0.664}$.

FIG. 4. Plot of the power-law scaling exponent α of the minimum neck radius R_{min} vs the density ratio D. Error bars represent a 95% confidence interval. There is a sharp transition from $\alpha \approx 0.57$ to $\alpha \approx 2/3$ when the density ratio is near 0.25 (dotted line). This transition represents a bifurcation of the solutions of the equations of motion from bubblelike to droplet-like pinch-off.

[4,7] and the corresponding similarity solutions [4] show that the power law $R_{min} \sim (t_0 - t)^{2/3}$ is valid for a range of values of D. However, for $D \leq 0.16$, the numerical solutions become linearly unstable to oscillatory modes, producing striking fractal-like shapes near pinch-off. These simulations do not address density ratios below 0.16 due to the high computational costs of resolving the fine structure in shapes with high curvature. Experimentally, at these intermediate density ratios [Fig. 2(c)], we see no evidence of this oscillatory instability; the fluid profile evolves smoothly from the sharply pointed filament characteristic of drops to the hyperboloids characteristic of bubbles. Although it is possible that this instability may occur under the optical horizon of the drop at small length scales, we believe that the viscous boundary-layer of gas at the free surface (which is not accounted for in the inviscid simulations) damps out any oscillatory behavior. Numerical techniques have also been used to study the bubblelike regime for $D < 0.01$ [13,14,21]. The results show that the exponent α is independent of D at sufficiently long times, but at extremely short times and high Reynolds numbers a crossover to $\alpha = 1/3$ is expected; apparently this regime is outside the dynamical range of our experiment.

In conclusion, we have observed the transition from bubble to droplet pinch-off using xenon rising in water at pressures up to 68 atm. The behavior of the minimum neck radius R_{min} is determined by the density ratio $D = \rho_{int}/\rho_{ext}$. Assuming a power law of the form $R_{min} \sim (t_0 - t)^{\alpha}$, the scaling exponent α is approximately constant $\alpha \approx 0.57$ for $D < 0.1$, while $\alpha \approx 2/3$ for all $D > 0.25$. The bubble and dropletlike regimes represent stable fixed points of the dynamical system. The transition between the two fixed points is quite abrupt, and is probably related to the inviscid instabilities discussed in Ref. [4], broadened by weak viscous and boundary-layer effects.

[1] J. Eggers and E. Villermaux, Rep. Prog. Phys. **71**, 036601 (2008).
[2] Y.-J. Chen and P. Steen, J. Fluid Mech. **341**, 245 (1997).
[3] R. F. Day, E. J. Hinch, and J. R. Lister, Phys. Rev. Lett. **80**, 704 (1998).
[4] D. Leppinen and J. R. Lister, Phys. Fluids **15**, 568 (2003).
[5] J. C. Burton and P. Taborek, Phys. Fluids **19**, 102109 (2007).
[6] A. U. Chen, P. K. Notz, and O. A. Basaran, Phys. Rev. Lett. **88**, 174501 (2002).
[7] N. Monika and P. H. Steen, J. Comput. Phys. **200**, 299 (2004).
[8] J. C. Burton, J. E. Rutledge, and P. Taborek, Phys. Rev. E **75**, 036311 (2007).
[9] J. C. Burton, J. E. Rutledge, and P. Taborek, Phys. Rev. Lett. **92**, 244505 (2004).
[10] H. N. Oguz and A. Prosperetti, J. Fluid Mech. **257**, 111 (1993).
[11] M. S. Longuet-Higgins, B. R. Kerman, and K. Lunde, J. Fluid Mech. **230**, 365 (1991).
[12] J. C. Burton, R. Waldrep, and P. Taborek, Phys. Rev. Lett. **94**, 184502 (2005).
[13] J. M. Gordillo, A. Sevilla, J. Rodriguez-Rodriguez, and C. Martinez-Bazan, Phys. Rev. Lett. **95**, 194501 (2005).
[14] J. M. Gordillo and M. Perez-Saborid, J. Fluid Mech. **562**, 303 (2006).
[15] R. Bergmann, D. van der Meer, M. Stijnman, M. Sandtke, A. Prosperetti, and D. Lohse, Phys. Rev. Lett. **96**, 154505 (2006).
[16] J. Eggers, M. A. Fontelos, D. Leppinen, and J. H. Snoeijer, Phys. Rev. Lett. **98**, 094502 (2007).
[17] S. T. Thoroddsen, T. G. Etoh, and K. Takehara, Phys. Fluids **19**, 042101 (2007).
[18] N. C. Keim, P. Moller, W. W. Zhang, and S. R. Nagel, Phys. Rev. Lett. **97**, 144503 (2006).
[19] J. Eggers and M. A. Fontelos, arXiv:0711.0442.
[20] V. A. Galaktionov and J. Vazquez, *A Stability Technique for Evolution Partial Differential Equations: A Dynamical Systems Approach* (Birkhauser, Boston, 2003).
[21] J. M. Gordillo and M. A. Fontelos, Phys. Rev. Lett. **98**, 144503 (2007).
[22] Y. A. Dyadin, E. G. Larionov, D. S. Mirinskij, T. V. Mikina, E. Y. Aladko, and L. I. Starostina, J. Inclusion Phenom. Mol. Recognit. Chem. **28**, 271 (1997).
[23] E. W. Lemmon, M. O. McLinden, and D. G. Friend, in *NIST Chemistry WebBook, NIST Standard Reference Database Number 69*, edited by P. J. Linstrom and W. G. Mallard (National Institute of Standards and Technology, Gaithersburg, MD, 2005), http://webbook.nist.gov.
[24] Although this restriction is not very important in the case of low densities because the power-law solution persists to $(t_0 - t) \sim 1$ ms, at higher densities there is a characteristic knee in the data at $(t_0 - t) \sim 300$ μs that corresponds to the approach to the self-similar, asymptotic solution [Fig. 3(b), circles]. This knee has been observed in previous experimental measurements of inviscid droplet pinch-off in superfluid helium [8], and is explained in detail in [2].